



Wideband SOA fiber-to-fiber gain and saturation output power in the C-band: impact of characteristic parameters

Arwa Hassan Beshr¹ · Moustafa H. Aly²

Received: 16 January 2023 / Accepted: 20 March 2023 / Published online: 8 April 2023
© The Author(s) 2023

Abstract

Semiconductor Optical Amplifiers (SOAs) have numerous attractive characteristics; for example: minimum power usage, broadband, flexible wavelength, wide dynamic range and significant nonlinearities. In this study, we present a comprehensive model of output saturation power and fiber-to-fiber gain of wideband SOAs. Furthermore, we investigate the impact of optical confinement factor, bias current, input signal power, temperature, and amplifier length on the fiber-to-fiber gain spectrum in the C-band. The obtained numerical results are approved by comparison with simulation results showing a fair agreement. The results reveal that output saturation power is improved by decreasing the optical confinement factor. Additionally, when input signal power rises, the maximum fiber-to-fiber gain value declines. Furthermore, as the temperature rises, the fiber-to-fiber gain decreases. Moreover, the maximum fiber-to-fiber gain is obtained at shorter amplifier lengths. Additionally, the effect of carrier density on the spectrum of coefficient of material gain is investigated, showing an increase in its value when increasing the carrier density, with a peak near 1550 nm.

Keywords SOA · Fiber-to fiber gain · Output power saturation · Bias current · Input signal power · Temperature · Amplifier length

1 Introduction

The SOAs technology has become increasingly important for the use, improvement, and optimization of photonic circuits, networks, and subsystems in recent years (Zoiros 2018, Volet et al. 2017 and Perin et al. 2016). The SOAs demonstrate numerous fundamental characteristics, such as broad band, significant nonlinearities, wide dynamic range, minimum power consumption, flexible range of wavelengths, rapid response, varied operations

✉ Moustafa H. Aly
mosaly@aast.edu

Arwa Hassan Beshr
arwabeshr@gmail.com

¹ High Institute for Computer and Information Systems, Alexandria, Egypt

² College of Engineering and Technology, Arab Academy for Science, Technology and Maritime Transport, Alexandria, Egypt

and small footprint (Pleros et al. 2007). These desirable characteristics have made the SOAs essential elements to accomplish the major and at fundamentally critical tasks (Rizou et al. 2017). Despite all these desirable characteristics, the usage of SOAs is quite restricted in linear amplification systems, however there is utilize of SOAs in such applications (Bonk et al. 2012).

One of the major limitation of SOAs is its low output saturation power, P_{sat} . There are many methods to improve the output saturation power including decreasing the optical confinement factor (Brenot et al. 2005), the use of flared waveguides (Bendelli et al. 1991), gain clamping (Giuliani and D’Alessandro 2000), and pump beams (Yoshino and Inoue 1996).

Recently, high efficient, high gain, and high saturation output power quantum-dot SOAs grown on Si and its applications are demonstrated by Liu et al. (2020). Moreover, the fundamental study of saturation output power on quantum-dot SOA under high temperature was presented by Kuwahata et al. (2019). Additionally, the characterization of the wide-band semiconductor optical amplifier was investigated by Beshr et al. numerically and by simulation (Beshr and Aly 2023).

In this paper, we present a comprehensive model of output saturation power and fiber-to-fiber gain of wideband SOAs. We investigate the effects of optical confinement factor and bias current on improving the output power saturation and fiber-to-fiber gain, Moreover, we study the impact of bias current, input signal power, temperature, and amplifier length on the fiber-to-fiber gain spectrum in the C-band. The obtained numerical results show a good accordance with the ones obtained by simulation.

The format of this paper is as follows. In Sect. 2, a comprehensive model of output saturation power and fiber-to-fiber gain of wideband SOAs is described. Section 3 presents and discusses the numerical results, including comparisons between numerical and simulation approaches. Section 4 is dedicated to main conclusions.

2 Mathematical model

2.1 Improvement of output power saturation

One of the major characteristics of SOA is the high output power saturation; mainly for power booster and multichannel applications. A simple rate equation model is utilized to define the parameters that affect SOA gain at high input power. At the signal wavelength, the coefficient of material gain, g_m , is thought to be a linear function of carrier density, n , such as

$$g_m = a_1(n - n_0) \tag{1}$$

where a_1 is the differentiation of g_m with respect to n , n_0 is the transparency carrier density.

The coefficient of material gain g_m (m^{-1}) showing the bulk-material active area of InGaAsP with direct bandgap as a function of wavelength of the signal is determined as (Connelly 2001).

$$g_m(\lambda, n) = \frac{\lambda^2}{4\sqrt{2\pi}^{3/2}n_{eq}\tau} \left(\frac{2m_e m_{hh}}{\hbar(m_e + m_{hh})} \right)^{3/2} \chi \sqrt{\frac{c}{\lambda} - \frac{E_{go} - \Delta E_g(n)}{h}} (f_c(\lambda) - f_v(\lambda)) \tag{2}$$

where m_{hh} stands for the effective mass of the heavy hole in the valance band and m_e stands for the effective mass of the electron in the conduction band. The probability distributions of Fermi–Dirac for conduction and valance band are denoted by $f_c(\lambda)$ and $f_v(\lambda)$, correspondingly, E_{g0} , the no carrier injection bandgap energy, $\Delta E_g(n)$ is the shrinkage band-gap caused by injection (Adachi 1992).

The carrier density rate equation

$$\frac{dn}{dt} = \frac{J}{ed} - \frac{n}{\tau} - a_1(n - n_0) \frac{I_s}{h\nu} \quad (3)$$

The travelling-wave equation describes how the signal intensity, I_s , moves across the SOA

$$\frac{dI_s}{dz} = [\Gamma a_1(n - n_0) - \alpha] I_s \quad (4)$$

where the time is denoted by t , z is the direction of propagation, J stands for the active region's current density, e for the electron's charge, d for the thickness of the active region, τ for the lifespan of the spontaneous carrier, h for Planck's constant, ν for the optical signal's frequency, and α for the coefficient of waveguide loss.

The output power saturation is well-described as the output power obtained by the SOA when the gain is decreased by 3 dB.

The output power saturation is determined by (Connelly 2007)

$$P_{sat} = \frac{A I_{sat,out}}{\Gamma} \quad (5)$$

where A represents the size of the active region, Γ stands for confinement factor, and $I_{sat,out}$ represents the saturation output intensity, given by (Connelly 2007)

$$I_{sat,out} = \frac{\ln(2) G_0 I_{sat}}{G_0 - 2} \quad (6)$$

The unsaturated gain, G_0 is defined as (Connelly 2007)

$$G_0 = \exp(\Gamma g_0 L) \quad (7)$$

where the intensity of saturation, I_{sat} , and the power of saturation, P_{sat} , are determined respectively, as

$$I_{sat} = \frac{h\nu}{a_1 \tau} \quad (8)$$

$$P_{sat} = \frac{A I_{sat}}{\Gamma} \quad (9)$$

where L is the amplifier length and g_0 is the coefficient of unsaturated material gain.

2.2 Fiber to fiber gain of SOA

The intrinsic gain, G , taking into account coupling losses at the input and output is referred to as the fiber to fiber gain, $G(\nu)$, at the optical frequency ν .

Table 1 Material parameters and geometrical used in simulation (M.J. Connelly 2001)

Symbol	Parameter	Value
d	Active region thickness	0.4 μm
Γ	Optical confinement factor	0.45
L	Amplifier length	700 μm
m_e	Effective mass of electron in the conduction band	4.10×10^{-32} kg
m_{hh}	Effective mass of a heavy hole in the valence band	4.19×10^{-31} kg
T	SOA absolute temperature	300 K

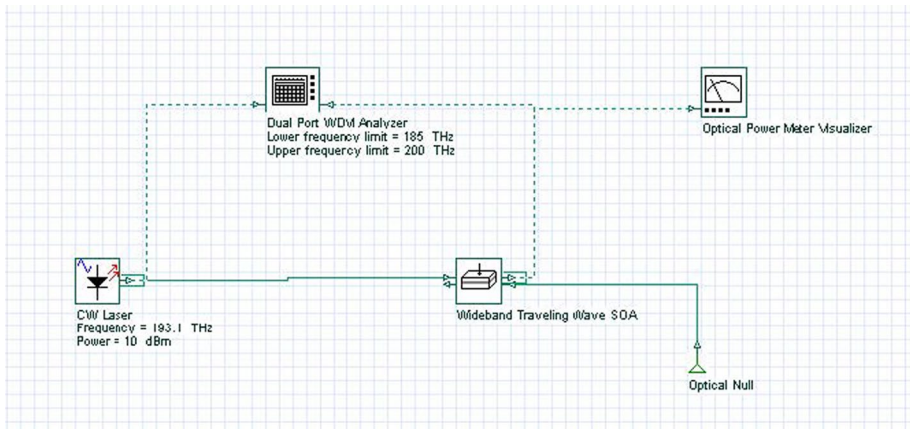


Fig. 1 Setup configuration using OptiSystem

The fiber to fiber gain at the optical frequency, ν , is given by (Connelly 2001)

$$G_s(\nu) = \exp \left\{ \int_0^L [g_m(\nu, n) - \alpha(n)] dz \right\} \tag{10}$$

where $\alpha(n)$ is the coefficient of material loss (Connelly and O’Dowd 1995).

3 Results and discussion

In this section, we present the numerical findings from MATLAB and compare them with the simulation results that are performed by OptiSystem. An excellent accordance is achieved between numerical and simulation results. Table 1 shows the material parameters and geometrical for the SOA use in this simulation.

The setup configuration, used in simulation, is built using OptiSystem as shown in Fig. 1.

Fig. 2 Relationship between numerical fiber-to-fiber gain and output power at various confinement parameters (using MATLAB)

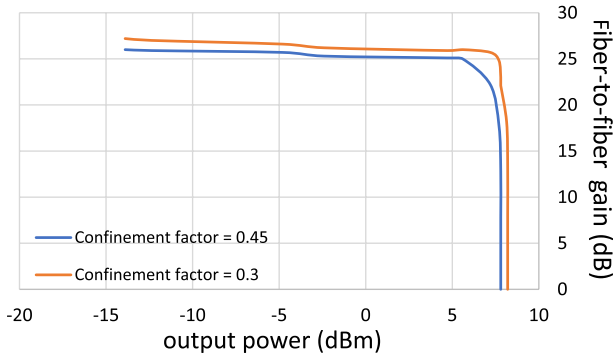
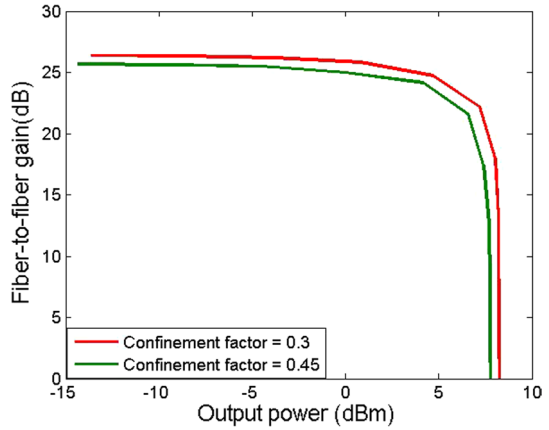


Fig. 3 Simulated fiber-to-fiber gain as a function of output power at various confinement parameters (using OptiSystem)

3.1 Output power saturation: impact of confinement factor

As a function of output power saturation at various optical confinement factors, the numerical and simulated fiber to fiber gain is provided in Figs. 2, 3, respectively, at.

1550 nm input signal wavelength and 150 mA bias current.

It is noticed that, the amplifier with small optical confinement factor, Γ , exhibits high output power saturation as predicted from Eq. (4). At a small confinement factor of 0.3, the peak gain numerically achieved is ~ 26.3 dB and the output power saturation is 8.21 dBm. This compares favorably to the equivalent stimulated maximum gain of 26.9 dB and the output power saturation is 8.2 dBm.

At higher confinement factor, 0.45, the numerically maximum gain achieved is ~ 25.6 dB and the output power saturation is decreased to 7.74 dBm. This compares approvingly to the corresponding stimulated value (~ 26 dB) when the output power saturation is decreased to 7.8 dBm.

Fig. 4 Relationship between numerical fiber- to-fiber gain and output power at various bias currents (using MATLAB)

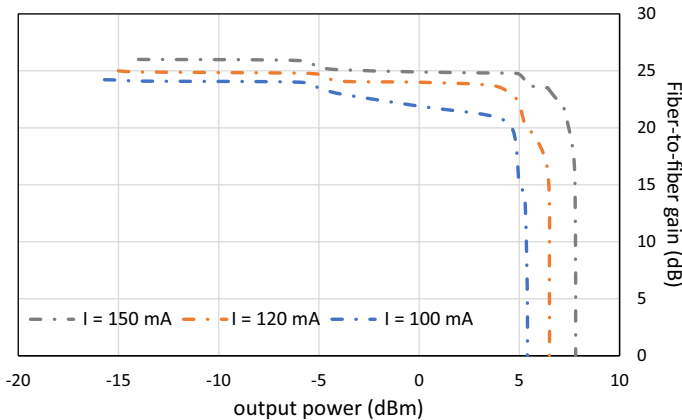
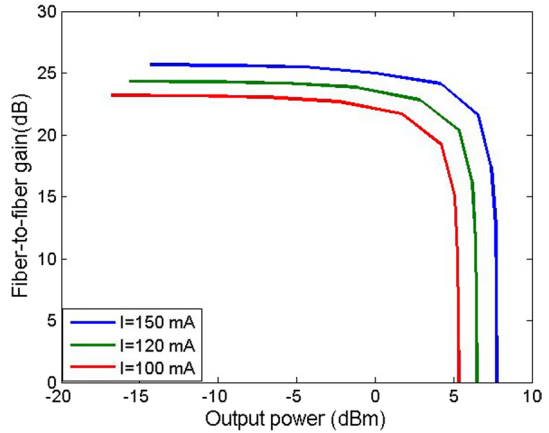


Fig. 5 Simulated fiber-to-fiber gain with respect to output power at various bias currents (using OptiSystem)

3.2 Output power saturation: impact of bias current

Figures 4, 5 show, respectively, the numerical and simulated gain saturation characteristics of SOA as a function of output power. The function of output power saturation is used to illustrate the numerical and simulated fiber to fiber gain for the assigned bias currents 100, 120 and 150 mA with 1550 nm input signal wavelength.

At a higher bias current of 150 mA, the numerical and simulated maximum gain obtained are 25.6 dB and 25.9 dB, and the output power saturation values are 7.744 dBm and 7.8 dBm, respectively, showing an excellent agreement.

At 100 mA (low bias current), the numerical and simulated maximum gain obtained are 23.2 dB and 24 dB, and the output power saturation values are reduced to 5.3 dBm and 5.4 dB, respectively. Again, this reveals an excellent agreement between numerical analysis and simulation. Evidently, an improvement of the output power from 5.4 to 7.8 dBm are predicted from Eq. (4) by improving the bias current from 100 to 150 mA.

Fig. 6 Numerical gain spectrum at different bias current (using MATLAB)

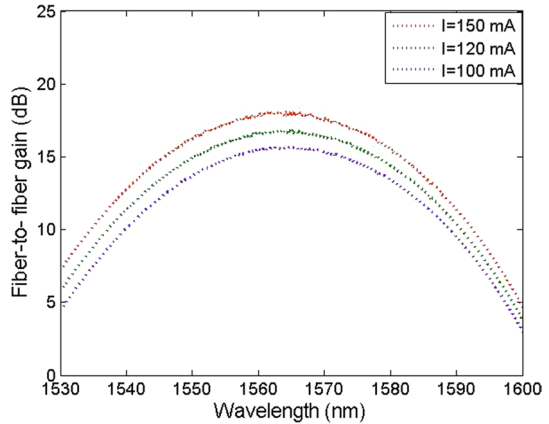
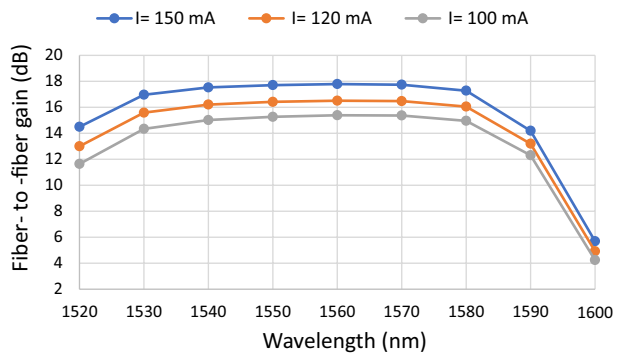


Fig. 7 Simulated fiber-to-fiber gain spectrum at multiple bias currents (using OptiSystem)



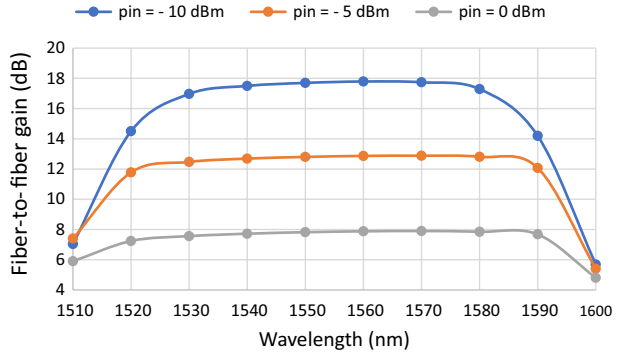
3.3 Fiber-to-fiber gain spectrum: impact of bias current

We introduce the effect of input bias current on the improving the fiber-to-fiber gain spectrum for C-band at power of input signal—10 dBm in Figs. 6, 7, numerically and by simulation, respectively. The bias current, I , is assigned values of 150, 120 and 100 mA. It is noticed that, the fiber to fiber gain improving with increasing the bias current, until getting its maximum value at ~ 1565 nm, then decreases. As shown, the SOA optical gain spectrum is very diverse. Clearly, the maximum gain increases also with the bias current. The discrepancy between both the numerical and simulation results is insignificant showing a fair agreement.

3.4 Fiber-to-fiber gain spectrum: impact of input signal power

Assigned signal powers of -10 , -5 , and 0 dBm in the C-band at an input bias current of 150 mA are presented in Fig. 8 along with the simulated fiber-to-fiber gain. Evidently, increasing the power of input signal leads to a decrease in the fiber-to-fiber gain. This can be explained as follows. As the signal power rises, the number of carriers in the active zone decreases, which causes the gain to fall and the wavelengths to shift

Fig. 8 Simulated spectrum of fiber-to-fiber gain at various input signal powers (using OptiSystem)



towards longer ones. The maximum obtained gain of 17.7, 12.8, and 7.8 dB at -10 , -5 and 0 dBm input signal power of, respectively, at 1550 nm wavelength.

3.5 Fiber to fiber gain spectrum: impact of temperature

Figure 9 displays the simulated SOA fiber-to-fiber gain spectrum at multiple temperatures, T, 220, 250 and 300 K, at 150 mA bias current and -10 dBm input signal power.

It was observed that as the temperature rose, the fiber-to-fiber gain decreased. This is because at high temperatures, the electron distribution spans a greater energy range. As a result, there are less electrons accessible at a given energy to take part in an optical transition, which results in a gain. This result is in a fair agreement with work of Dutta and Wang (2013). Clearly, the maximum gain is achieved at 1550 nm and then reduces towards longer wavelengths when temperature is increased.

3.6 Fiber-to-fiber gain spectrum: impact of amplifier length

Figure 10 displays the simulated gain spectrum at multiple amplifier lengths, L= 600, 700 and 800 μm , at 150 mA bias current and -10 dBm input signal power. We observe that, the fiber-to-fiber gain falls with increased amplifier lengths.

The maximum gain, 18.55, 17.71, and 16.95 dB is obtained at amplifier lengths of 600, 700, and 800 μm , respectively, at 1550 nm wavelength.

Fig. 9 Simulated gain spectrum at different temperatures, at 150 mA bias current and -10 dBm input signal power (using OptiSystem)

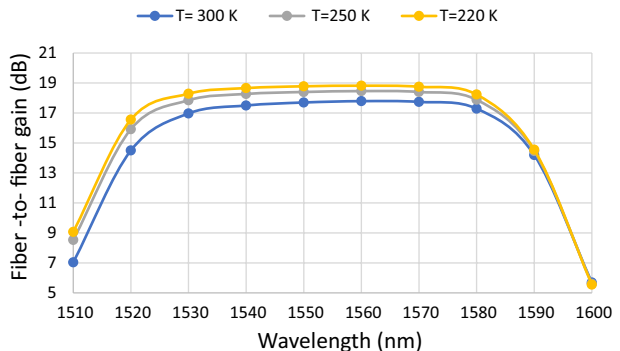


Fig. 10 Simulated gain spectrum at multiple amplifier lengths, L , at input signal power = -10 dBm and bias current = 150 mA (using OptiSystem)

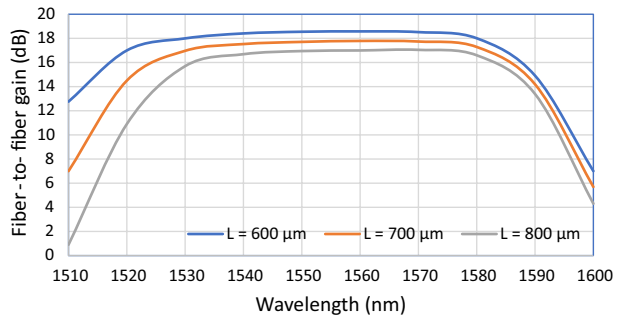
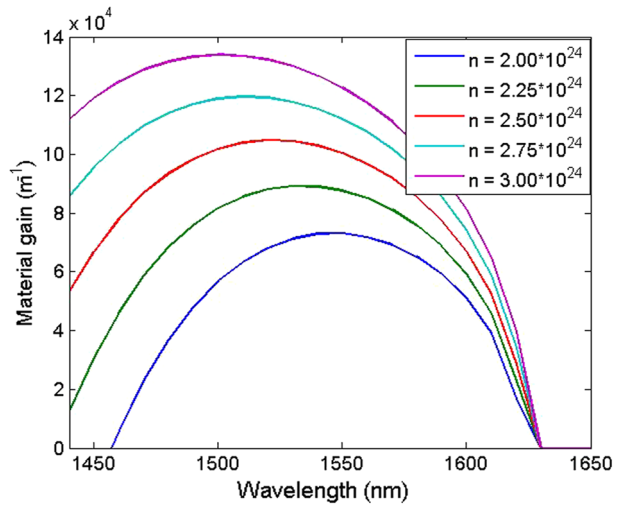


Fig. 11 The coefficient of material gain at different values of carrier density, n , in the C-band



3.7 The coefficient of material gain spectrum: impact of carrier density

Figure 11 displays the coefficient of material gain versus carrier density, n , in the C-band. Clearly, the coefficient of material gain increases with the carrier density, showing a peak at 1550 nm, which is in a fair agreement with the work of Agrawal et al. (2022).

4 Conclusion

The saturation output power and fiber-to-fiber gain of wideband SOAs are discussed in length in this study. Bias current and optical confinement factor effects are examined numerically and through simulation. It is discovered that raising the bias current and lowering the confinement factor improve fiber-to-fiber gain and output power saturation. The maximum gain and output power saturation obtained are 25.9 dB and 7.8 dBm, respectively, at 150 mA (high bias current). While the minimum gain and output power saturation achieved are 24 dB and 5.4 dBm, respectively, at 100 mA (low bias current). Also, the output power saturation is improved from 7.8 to 8.2 dBm by decreasing the

optical confinement factor from 0.45 to 0.3. The numerical results are validated by simulated ones, showing excellent agreement.

Moreover, we studied the impact of input signal power, temperature and amplifier length on the fiber-to-fiber gain spectrum. A maximum gain of 17.7, 12.8 and 7.8 dB is obtained at an input signal power of -10 , -5 and 0 dBm, respectively, at 1550 nm wavelength. Additionally, the fiber-to-fiber gain falls with increasing the temperature and the maximum gain is achieved at 220 K, at 1550 nm wavelength. Moreover, the maximum fiber-to-fiber gain, 18.55 dB, is obtained at minimum amplifier length of 600 μm at 1550 nm wavelength. We also studied the impact of the carrier density on coefficient of material gain spectrum, where the coefficient of material gain peaks near 1550 nm and gets better as the carrier density rises. Finally, the discrepancy among both the numerical and simulation results is insignificant showing a fair agreement.

Author contributions AHB and MHA have directly participated in the planning, execution, and analysis of this study. AHB. drafted the manuscript. All authors have read and approved the final version of the manuscript.

Funding Open access funding provided by The Science, Technology & Innovation Funding Authority (STDF) in cooperation with The Egyptian Knowledge Bank (EKB). The authors did not receive any funds to support this research.

Data availability The data used and/or analyzed during the current study are available from the corresponding author on reasonable request.

Declarations

Conflict of interest The authors declare that they have no competing interests.

Ethical approval Not Applicable.

Open Access This article is licensed under a Creative Commons Attribution 4.0 International License, which permits use, sharing, adaptation, distribution and reproduction in any medium or format, as long as you give appropriate credit to the original author(s) and the source, provide a link to the Creative Commons licence, and indicate if changes were made. The images or other third party material in this article are included in the article's Creative Commons licence, unless indicated otherwise in a credit line to the material. If material is not included in the article's Creative Commons licence and your intended use is not permitted by statutory regulation or exceeds the permitted use, you will need to obtain permission directly from the copyright holder. To view a copy of this licence, visit <http://creativecommons.org/licenses/by/4.0/>.

References

- Adachi, S.: Physical properties of III IV semiconductor compounds. Wiley, New York (1992)
- Agrawal, G.P., Sobhanan, A., Aravind, A., Sean, O., Mark, P., Shu, N., Liam, B., Deepa, V.: Semiconductor optical amplifiers: recent advances and applications. *Adv. Opt. Photonics*. **14**(3), 571–651 (2022)
- Bendelli, G., Komori, K., Arai, S., Suematsu, Y.: A new structure for high-power TW-SLA. *IEEE Photon Technol. Lett.* **3**(1), 42–44 (1991)
- Beshr, A.H., Aly, M.H.: Characterization of wideband semiconductor optical amplifier: numerical analysis and simulation. *Opt. Quantum. Electron.* **55**, 287 (2023). <https://doi.org/10.1007/s11082-023-04575-5>
- Bonk, R., Huber, G., Vallaitis, T., Koenig, S., Schmogrow, R., Hillerkuss, D., Brenot, R., Lelarge, F., Duan, G.H., Sygletos, S., Koos, C., Freude, W., Leuthold, J.: Linear semiconductor optical amplifiers for amplification of advanced modulation formats. *Opt. Express* **20**(9), 9657–9672 (2012)

- Brenot, R., Pommereau, F., Le Gouez, O., Landreau, J., Poingt, F., Le Gouezigou, L., Rousseau, B., Lelarge, F., Martin, F., Duan, G.H.: Experimental study of the impact of optical confinement on saturation effects in SOA. In: Optical fiber communications conference (OFC 2005) Paper OME50 (2005)
- Connelly, M.J.: Wideband semiconductor optical amplifier steady-state numerical model. *IEEE J. Quantum Electron.* **37**(3), 439–447 (2001)
- Connelly, M.J.: Semiconductor optical amplifiers. Springer, Berlin (2007)
- Connelly, M.J., O'Dowd, R.F.: Travelling-wave semiconductor optical amplifier detector noise characteristics. *IEE Proc. Optoelectron* **142**(1), 23–28 (1995)
- Dutta, N.K., Wang, Q.: Semiconductor optical amplifiers. World Scientific, Singapore (2013)
- Giuliani, G., D'Alessandro, D.: Noise analysis of conventional and gain-clamped semiconductor optical amplifiers. *J. Lightwave Technol.* **18**(9), 1256–1263 (2000)
- Kuwahata, R., Jiang, H., Hamamoto, K.: Fundamental study of saturation output power on quantum dot semiconductor optical amplifier under high temperature (85 °C). In: the 2019 IEEE 24th microoptics conference (MOC), pp. 180–181 (2019)
- Liu, S., Tong, Y., Norman, J., Dumont, M., Gossard, A., Tsang, H.K., Bowers, J.: High efficiency, high gain and high saturation output power quantum dot SOAs grown on Si and applications. In: 2020 optical fiber communications conference and exhibition (OFC), pp. 1–3 (2020) San Diego, CA
- Perin, J.K., Sharif, M., Kahn, J.M.: Sensitivity improvement in 100 Gb/s per wavelength links using semiconductor optical amplifiers or avalanche photodiodes. *J. Lightwave Technol.* **34**(23), 5542–5553 (2016)
- Pleros, N., Zakyntinos, P., Poustie, A., Tsiokos, D., Bakopoulos, P., Petranonakis, D., Kanellos, G.T., Maxwell, G., Avramopoulos, H.: Optical signal processing using integrated multi-element SOA–MZI switch arrays for packet switching. *IET Optoelectron.* **1**(3), 120–126 (2007)
- Rizou, Z.V., Zoiros, K.E.: Semiconductor optical amplifier dynamics and pattern effects. In: Joachim, P. (ed.) Handbook of optoelectronic device modeling and simulation, pp. 771–796. CRC Press, Boca Raton (2017)
- Volet, N., Spott, A., Stanton, E.J., Davenport, M.L., Chang, L., Peters, J.D., Briles, T.C., Vurgaftman, I., Meyer, J.R., Bowers, J.E.: Semiconductor optical amplifiers at 2.0 μm wavelength on silicon. *Laser Photonics Rev.* **11**, 1600165 (2017). <https://doi.org/10.1002/lpor.201600165>
- Yoshino, M., Inoue, K.: Improvement of saturation output power in a semiconductor laser amplifier through pumping light injection. *IEEE Photon. Technol. Lett.* **8**(1), 58–59 (1996)
- Zoiros, E.: Special issue on applications of semiconductor optical amplifiers. *Appl. Sci.* **8**(7), 1–4 (2018)

Publisher's Note Springer Nature remains neutral with regard to jurisdictional claims in published maps and institutional affiliations.